

Can we determine the NME of NLDBD with the data of other observables?

Jiangming Yao (尧江明)
中山大学物理与天文学院
School of Physics and Astronomy
Sun Yat-sen University

Journal Club, Nuclear Physics Group

Sep, 2022

Abstract

中山大學 SUN YAT-SEN UNIVERSITY

A Statistical Analysis for the Neutrinoless Double-Beta Decay Matrix element of ^{48}Ca

M. Horoi,[1] A. Neacsu,[2] and S. Stoica[2]

[1] *Department of Physics, Central Michigan University, Mount Pleasant, MI 48859, USA*
[2] *International Center for Advanced Training and Research in Physics (CIFRA), Magurele, Romania*

(Dated: March 22, 2022)

Neutrinoless double beta decay ($0\nu\beta\beta$) nuclear matrix elements (NME) are the object of many theoretical calculation methods, and are very important for analysis and guidance of a large number of experimental efforts. However, there are large discrepancies between the NME values provided by different methods. In this paper we propose a statistical analysis of the ^{48}Ca $0\nu\beta\beta$ NME using the interacting shell model, emphasizing the range of the NME probable values and its correlations with observables that can be obtained from the existing nuclear data. Based on this statistical analysis with three independent effective Hamiltonians we propose a common probability distribution function for the $0\nu\beta\beta$ NME, which has a range of (0.45 - 0.95) at 90% confidence level of, and a mean value of 0.68.

https://arxiv.org/abs/2203.10577

Introduction

It would be thus interesting to study the robustness of the $0\nu\beta\beta$ NME to small changes of the parameters of different effective shell model Hamiltonians and to examine how the NME changes are correlated with other observables. In this work, we propose a statistical analysis of $0\nu\beta\beta$ NME of ^{48}Ca calculated with the interacting shell-model using three independent effective Hamiltonians (FPD6, GXPF1A, KB3G), emphasizing the range of the NME probable values and their correlations with several observables that can be compared to existing nuclear data. Based on this statistical analysis we propose a common probability distribution function for the $0\nu\beta\beta$ NME. We apply our analysis to ^{48}Ca, which is the lightest DBD isotope and thus more accessible to ab-initio calculations. We only consider in this work the standard light LH neutrino exchange mass mechanism, which is most likely to contribute to the $0\nu\beta\beta$ decay process.

Introduction

The main goals are: (i) for each starting effective Hamiltonian find correlations between $0\nu\beta\beta$ NME and the other observables that are accessible experimentally; (ii) find theoretical ranges for each observables; (iii) establish the shape of different distributions for each observables and starting Hamiltonians; (iv) use this information to find weights of contributions from different starting Hamiltonians to the "optimal" distribution of the $0\nu\beta\beta$ NME; (v) find an "optimal" value of the $0\nu\beta\beta$ NME and its predicted probable range (theoretical error). One should mention that similar studies for other observables were recently proposed [49].

[49] J. M. R. Fox, C. W. Johnson, and R. N. Perez, Phys. Rev. C **101**, 054308 (2020).

The model

	Exp.	Error	FPD6	GXPF1A	KB3G
$0\nu\beta\beta$ NME	N/A	N/A	0.79	0.559	0.693
$2\nu\beta\beta$ NME	0.035 [38]	0.003	0.062	0.050	0.045
^{48}Ca B(E2)↑	0.008[39]	0.001	0.007	0.006	0.05
^{48}Ca 2+	3.832 [40]	0.15	3.658	3.735	4.238
^{48}Ca 4+	4.503 [40]	0.15	4.134	4.264	4.231
^{48}Ca 6+	7.953 [40]	0.15	7.396	7.705	7.831
^{48}Ca Occ(Nf5)	0.032^*	$0.395^\#$	0.117	0.032	0.112
^{48}Ca Occ(Nf7)	7.892^*	$0.395^\#$	7.693	7.892	7.795
^{48}Ca Occ(Np1)	0.009^*	$0.395^\#$	0.029	0.009	0.024
^{48}Ca Occ(Np3)	0.067^*	$0.395^\#$	0.161	0.067	0.070
^{48}Ca → ^{48}Sc GT	1.09 [41]	0.28	1.01	1.226	0.051
^{48}Ti B(E2)↑	0.063[39]	0.003	0.064	0.052	0.052
^{48}Ti 2+	0.984 [40]	0.150	1.118	1.010	0.985
^{48}Ti 4+	2.296 [40]	0.150	2.492	2.168	2.214
^{48}Ti 6+	3.333 [40]	0.150	3.425	2.922	3.046
^{48}Ti Occ(Nf5)	0.168^*	$0.277^\#$	0.310	0.168	0.263
^{48}Ti Occ(Nf7)	5.535^*	$0.277^\#$	5.253	5.535	5.416
^{48}Ti Occ(Np1)	0.048^*	$0.277^\#$	0.068	0.048	0.061
^{48}Ti Occ(Np3)	0.248^*	$0.277^\#$	0.369	0.248	0.260
^{48}Ti Occ(Pf5)	0.032^*	$0.092^\#$	0.101	0.032	0.097
^{48}Ti Occ(Pf7)	1.839^*	$0.092^\#$	1.672	1.839	1.763
^{48}Ti Occ(Pp1)	0.010^*	$0.092^\#$	0.031	0.010	0.021
^{48}Ti Occ(Pp3)	0.119^*	$0.092^\#$	0.196	0.119	0.120
^{48}Ti → ^{48}Sc GT	0.014[41]	0.005	0.050	0.032	0.056

Shell-model interactions

orbitals for both protons and neutrons), and added small random contributions to their two-body matrix elements (TBME). For this project we only considered the FPD6 Hamiltonian [42], the KB3G Hamiltonian [15], and GXPF1A Hamiltonian [43, 44] as starting effective Hamiltonians. In order to maintain the magicity of ^{48}Ca we decided to keep the single particle (s.p.) energies in the perturbed effective Hamiltonians the same as in the starting Hamiltonians.

fp-shell. An analysis of the TBME for all three starting Hamiltonians listed above indicates that a $\pm 10\%$ range for the random contributions would suffice.

Hamiltonian. For each starting effective Hamiltonian we use 20,000 random Hamiltonians produced by the procedure described in section II.

Results and discussion

Observable	Correlation	PDF
$0\nu\beta\beta$ NME	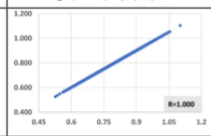	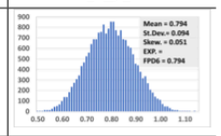
$2\nu\beta\beta$ NME	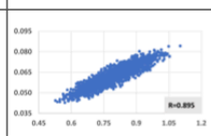	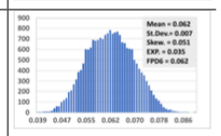
$^{48}\mathrm{Ca} \rightarrow {}^{48}\mathrm{Sc}$ GT	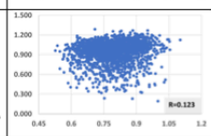	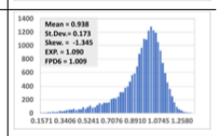
$^{48}\mathrm{Ti} \rightarrow {}^{48}\mathrm{Sc}$ GT	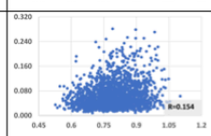	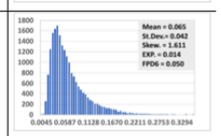
$^{48}\mathrm{Ca}$ B(E2)(↑)	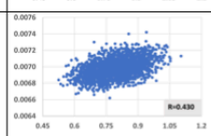	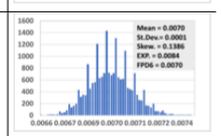
$^{48}\mathrm{Ca}\ 2^{+}$	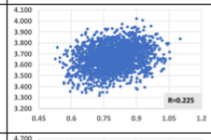	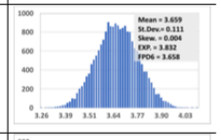
$^{48}\mathrm{Ca}\ 4^{+}$	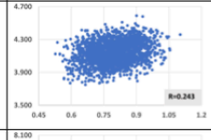	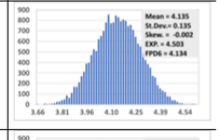
$^{48}\mathrm{Ca}\ 6^{+}$	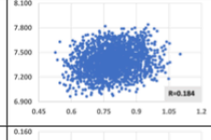	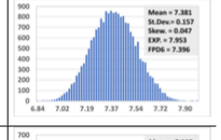
$^{48}\mathrm{Ca}$ Occ(Nf5)	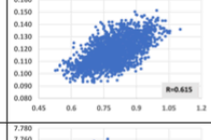	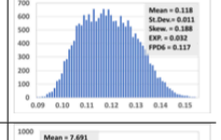
$^{48}\mathrm{Ca}$ Occ(Nf7)	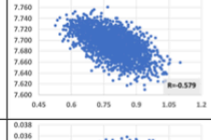	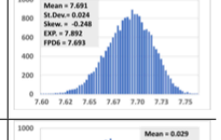
$^{48}\mathrm{Ca}$ Occ(Np1)	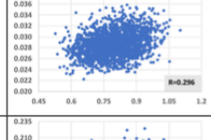	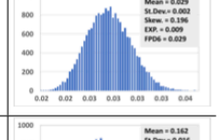
$^{48}\mathrm{Ca}$ Occ(Np3)	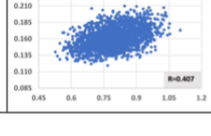	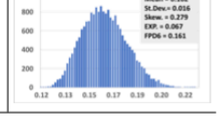

Observable	Correlation	PDF
$^{48}\mathrm{Ti}$ B(E2)(↑)	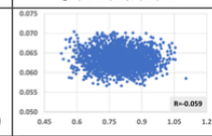	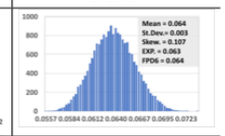
$^{48}\mathrm{Ti}\ 2^{+}$	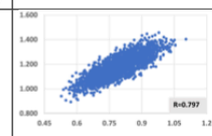	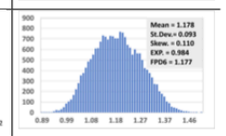
$^{48}\mathrm{Ti}\ 4^{+}$	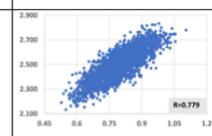	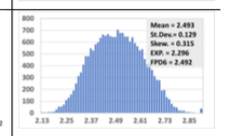
$^{48}\mathrm{Ti}\ 6^{+}$	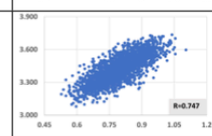	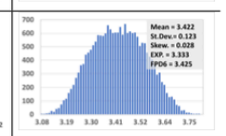
$^{48}\mathrm{Ti}$ Occ(Nf5)	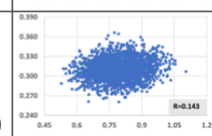	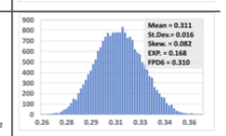
$^{48}\mathrm{Ti}$ Occ(Nf7)	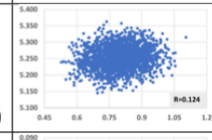	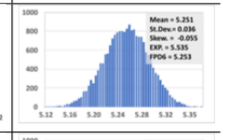
$^{48}\mathrm{Ti}$ Occ(Np1)	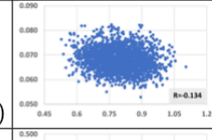	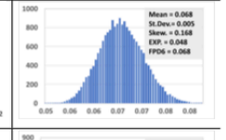
$^{48}\mathrm{Ti}$ Occ(Np3)	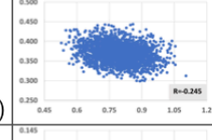	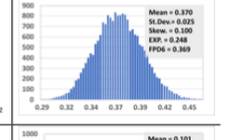
$^{48}\mathrm{Ti}$ Occ(Pf5)		
$^{48}\mathrm{Ti}$ Occ(Pf7)		
$^{48}\mathrm{Ti}$ Occ(Pp1)		
$^{48}\mathrm{Ti}$ Occ(Pp3)		

for the FPD6 starting Hamiltonian

Results and discussion

中山大學 SUN YAT-SEN UNIVERSITY

Observable	Correlation	PDF
$0\nu\beta\beta$ NME	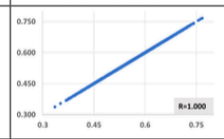	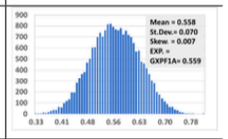
$2\nu\beta\beta$ NME	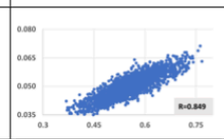	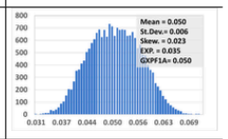
$^{48}\mathrm{Ca} \rightarrow {}^{48}\mathrm{Sc}$ GT	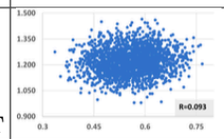	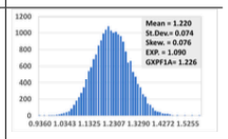
$^{48}\mathrm{Ti} \rightarrow {}^{48}\mathrm{Sc}$ GT	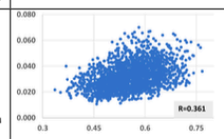	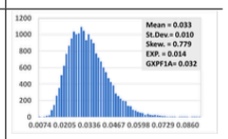
$^{48}\mathrm{Ca}$ B(E2)(↑)	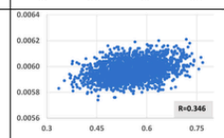	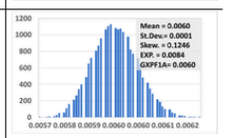
$^{48}\mathrm{Ca}$ 2^+	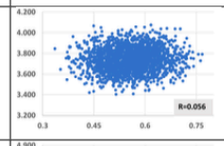	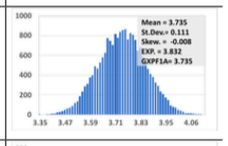
$^{48}\mathrm{Ca}$ 4^+	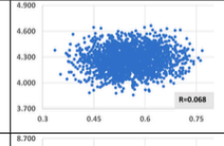	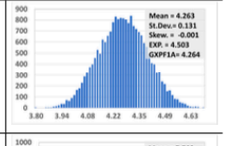
$^{48}\mathrm{Ca}$ 6^+	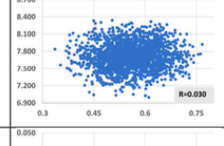	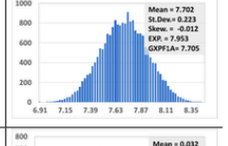
$^{48}\mathrm{Ca}$ Occ(Nf5)	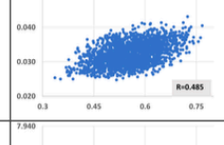	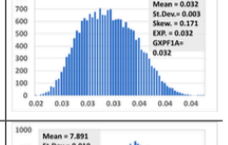
$^{48}\mathrm{Ca}$ Occ(Nf7)	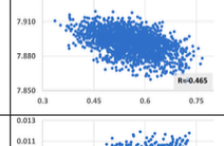	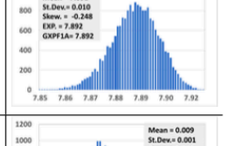
$^{48}\mathrm{Ca}$ Occ(Np1)	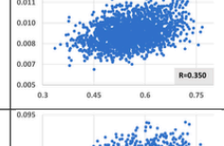	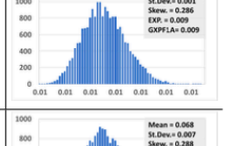
$^{48}\mathrm{Ca}$ Occ(Np3)	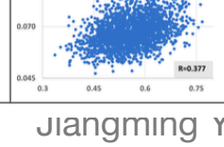	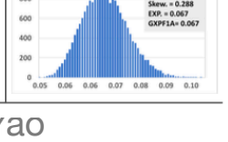

Observable	Correlation	PDF
$^{48}\mathrm{Ti}$ B(E2)(↑)	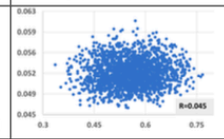	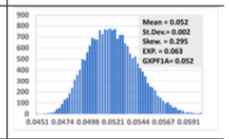
$^{48}\mathrm{Ti}$ 2^+	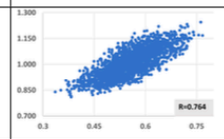	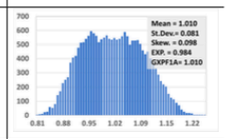
$^{48}\mathrm{Ti}$ 4^+	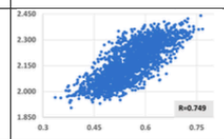	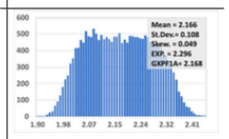
$^{48}\mathrm{Ti}$ 6^+	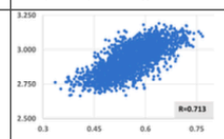	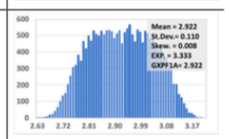
$^{48}\mathrm{Ti}$ Occ(Nf5)	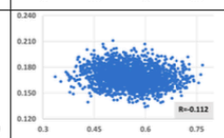	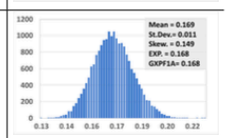
$^{48}\mathrm{Ti}$ Occ(Nf7)	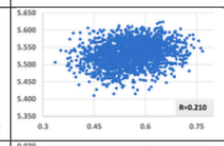	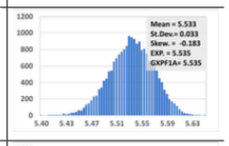
$^{48}\mathrm{Ti}$ Occ(Np1)	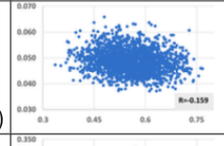	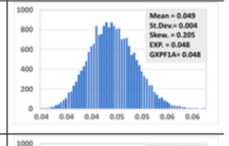
$^{48}\mathrm{Ti}$ Occ(Np3)	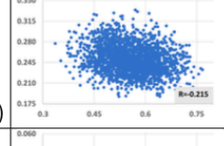	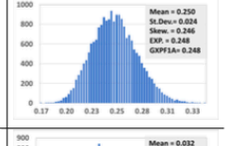
$^{48}\mathrm{Ti}$ Occ(Pf5)		
$^{48}\mathrm{Ti}$ Occ(Pf7)		
$^{48}\mathrm{Ti}$ Occ(Pp1)		
$^{48}\mathrm{Ti}$ Occ(Pp3)		

for the GXPF1A starting Hamiltonian

Results and discussion

Observable	Correlation	PDF
$0\nu\beta\beta$ NME	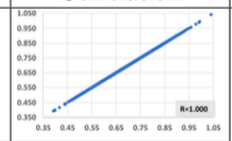	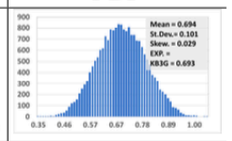
$2\nu\beta\beta$ NME	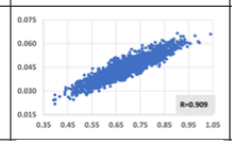	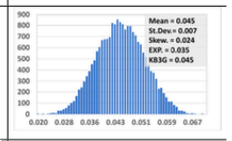
$^{48}\mathrm{Ca} \rightarrow {}^{48}\mathrm{Sc}$ GT	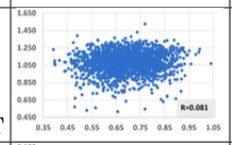	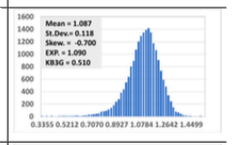
$^{48}\mathrm{Ti} \rightarrow {}^{48}\mathrm{Sc}$ GT	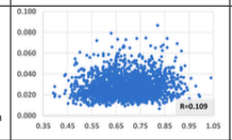	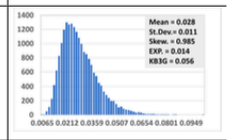
$^{48}\mathrm{Ca}$ B(E2)(↑)	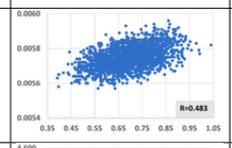	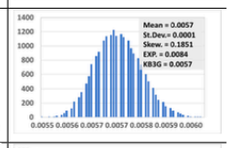
$^{48}\mathrm{Ca}$ 2^+	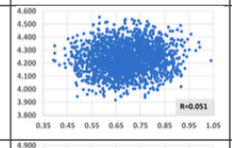	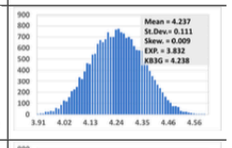
$^{48}\mathrm{Ca}$ 4^+	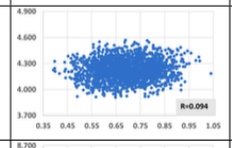	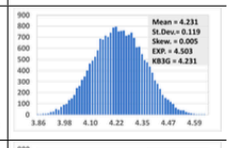
$^{48}\mathrm{Ca}$ 6^+	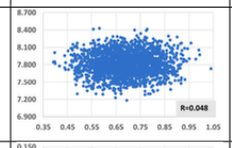	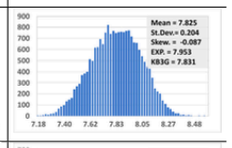
$^{48}\mathrm{Ca}$ Occ(Nf5)	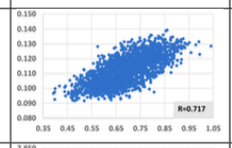	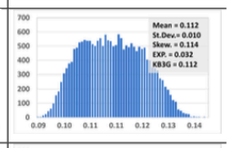
$^{48}\mathrm{Ca}$ Occ(Nf7)	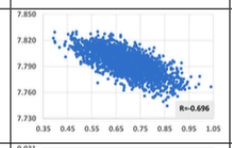	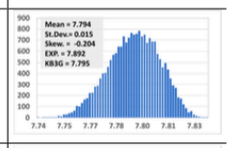
$^{48}\mathrm{Ca}$ Occ(Np1)	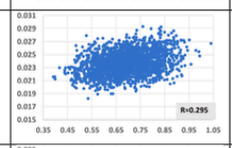	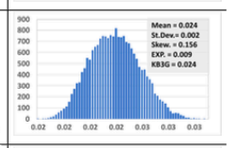
$^{48}\mathrm{Ca}$ Occ(Np3)	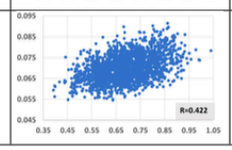	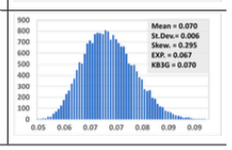

Observable	Correlation	PDF
$^{48}\mathrm{Ti}$ B(E2)(↑)	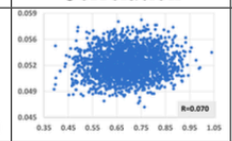	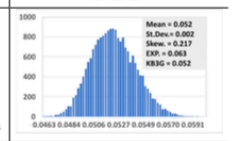
$^{48}\mathrm{Ti}$ 2^+	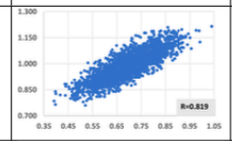	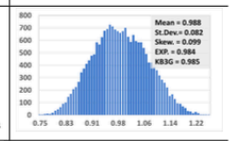
$^{48}\mathrm{Ti}$ 4^+	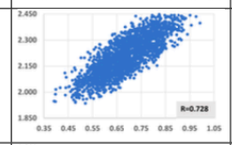	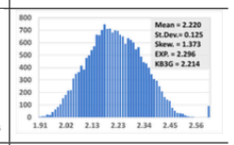
$^{48}\mathrm{Ti}$ 6^+	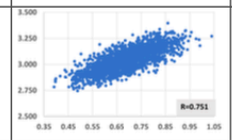	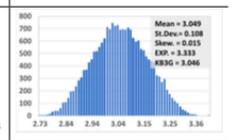
$^{48}\mathrm{Ti}$ Occ(Nf5)	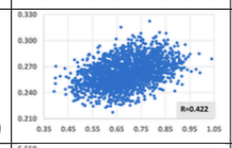	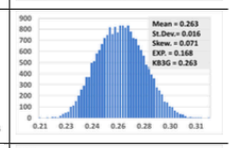
$^{48}\mathrm{Ti}$ Occ(Nf7)	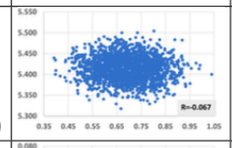	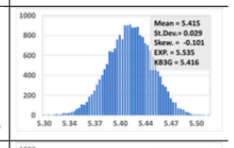
$^{48}\mathrm{Ti}$ Occ(Np1)	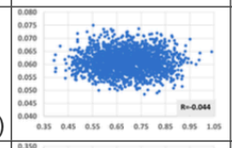	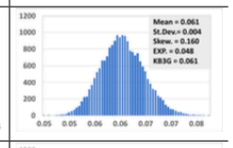
$^{48}\mathrm{Ti}$ Occ(Np3)	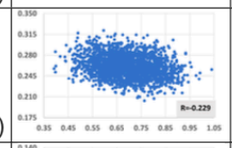	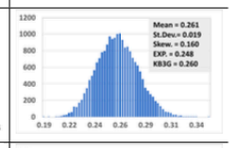
$^{48}\mathrm{Ti}$ Occ(Pf5)		
$^{48}\mathrm{Ti}$ Occ(Pf7)		
$^{48}\mathrm{Ti}$ Occ(Pp1)		
$^{48}\mathrm{Ti}$ Occ(Pp3)		

for the KB3G starting Hamiltonian

Results and discussion

In order to have a good representation for the PDF of the $0\nu\beta\beta$ NME, we consider small deviation from normal distribution via the Gram-Charlier A series [53]. This is given by:

$$P(x) \approx \frac{1}{\sqrt{2\pi}\sigma} exp\left[-\frac{(x-\mu)^2}{2\sigma^2}\right]$$
$$\cdot\left[1+\frac{\mu_3}{3!}He_3((x-\mu)/\sigma)+\frac{\mu_4-3}{4!}He_4((x-\mu)/\sigma)\right]$$

where $He_k(y)$ are the Chebyshev-Hermite polynomials, $He_3(y) = y^3 - 3y$ and $He_3(y) = y^4 - 6y^2 + 3$, μ and σ are the mean and variance of a probability density function (PDF), and μ_k, with $k = 3, 4$ are normalized moments of the same PDF, $P(x)$:

$$\mu_k = \int \left(\frac{x-\mu}{\sigma}\right)^k P(x)dx, \qquad (A.2)$$

In practice, we use the sample moments, μ_3 (skewnes) and $\mu_4 - 3$ (kurtosis), which in the limit of very large sample sizes become very close to the underlying moments.

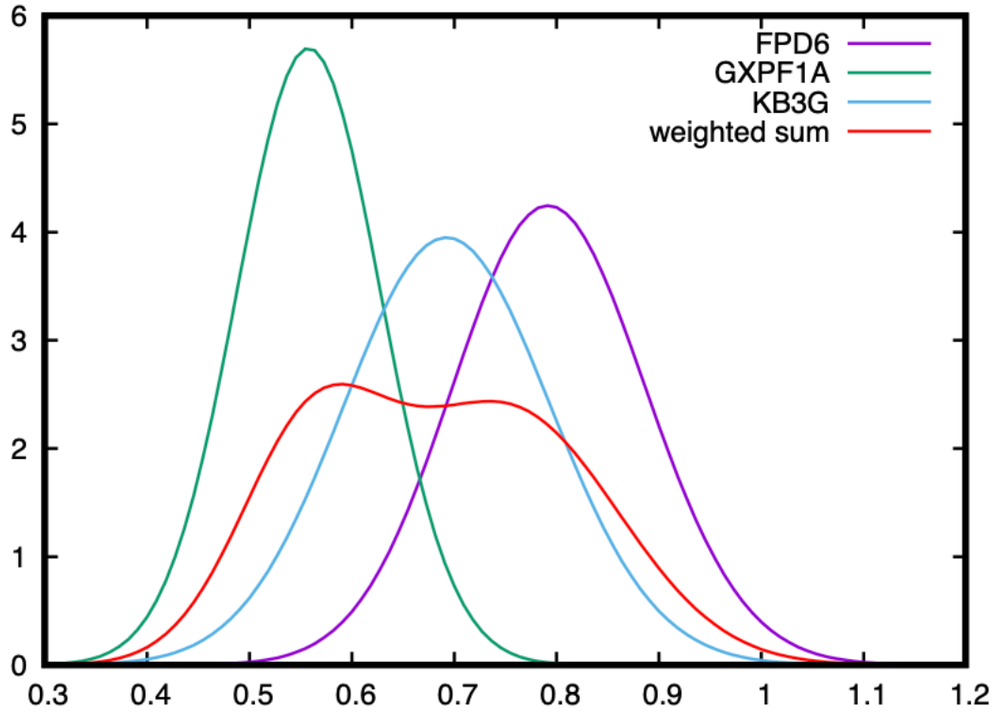

Figure 1. PDF of the $0\nu\beta\beta$ NME distributions for the FPD6, GXPF1A and KB3G Hamiltonians and their weighted sum (see text for details).

$$P(x) = W_{FPD6}P_{FPD6}(x) + W_{GXPF1A}P_{GXPF1A}(x) + W_{KB3G}P_{KB3G}(x) \ ,$$

here we present the results of a "democratic" approach in which all W_H are 0.33. Fig. 1 shows the probability distribution functions (PDF) for the three starting effective Hamiltonians and their weighted sum. To cal-

Summary

We found that the $0\nu\beta\beta$ NME correlates strongly with the $2\nu\beta\beta$ NME, but much less with the Gamow-Teller strengths to the first 1^+ state in ^{48}Sc. We also found that the $0\nu\beta\beta$ NME exhibits reasonably strong correlations with the energies of the 2^+, 4^+ and 6^+ states in ^{48}Ti, and with the neutron occupation probabilities in ^{48}Ca. We also found that there are additional correlations between observables, such as the energies of the 2^+, 4^+ and 6^+ states in ^{48}Ti and the neutron occupation probabilities, as well as between B(E2)$\uparrow$ values in ^{48}Ti and proton and neutron occupation probabilities, which can indirectly influence the $0\nu\beta\beta$ NME. Therefore, we conclude that reliable experimental values of the occupation probabilities in ^{48}Ti and ^{48}Ca would be useful for this analysis, potentially helpful to reduce the uncertainties of the $0\nu\beta\beta$ NME.

Based on this statistical analysis with three independent effective Hamiltonians we propose a common probability distribution function for the $0\nu\beta\beta$ NME, which has a range (theoretical error) of (0.45 - 0.95) at 90% confidence level, and a mean value of 0.68. We also hope that

Abstract

中山大學 SUN YAT-SEN UNIVERSITY

Neutrinoless $\beta\beta$-decay nuclear matrix elements from two-neutrino $\beta\beta$-decay data

Lotta Jokiniemi,[1,2,3,*] Beatriz Romeo,[4,†] Pablo Soriano,[1,2,‡] and Javier Menéndez[1,2,§]

[1] *Departament de Física Quàntica i Astrofísica, Universitat de Barcelona, 08028 Barcelona, Spain*
[2] *Institut de Ciències del Cosmos, Universitat de Barcelona, 08028 Barcelona, Spain*
[3] *TRIUMF, 4004 Wesbrook Mall, Vancouver, BC V6T 2A3, Canada*
[4] *Donostia International Physics Center, 20018 San Sebastián, Spain*

(Dated: July 13, 2022)

We study two-neutrino ($2\nu\beta\beta$) and neutrinoless double-beta ($0\nu\beta\beta$) decays in the nuclear shell model and proton-neutron quasiparticle random-phase approximation (pnQRPA) frameworks. Calculating the decay of several dozens of nuclei ranging from calcium to xenon with the shell model, and of $\beta\beta$ emitters with a wide range of proton-neutron pairing strengths in the pnQRPA, we observe good linear correlations between $2\nu\beta\beta$- and $0\nu\beta\beta$-decay nuclear matrix elements for both methods. We then combine the correlations with measured $2\nu\beta\beta$-decay half-lives to predict $0\nu\beta\beta$-decay matrix elements with theoretical uncertainties based on our systematic calculations. Our results include two-body currents and the short-range $0\nu\beta\beta$-decay operator.

https://arxiv.org/pdf/2207.05108.pdf

Introduction

The $2\nu\beta\beta$- and $0\nu\beta\beta$-decay half-lives depend on well-known phase-space factors [16] and nuclear matrix elements (NMEs) [17]. Additionally, $0\nu\beta\beta$ decay depends on a parameter encoding physics beyond the standard model of particle physics (BSM) leading to lepton-number violation. Hence, $0\nu\beta\beta$-decay NMEs are key to anticipate the reach of planned experiments in the BSM parameter space [18] and also to analyze eventual $0\nu\beta\beta$-decay signals. For $2\nu\beta\beta$ decay, NMEs can be extracted from measured half-lives [1], but NMEs for $0\nu\beta\beta$ decay are poorly known: differences between state-of-the-art calculations exceed a factor three and theoretical uncertainties are mostly ignored [3, 17].

Introduction

In this Letter, we study the correlation between the NMEs of the two $\beta\beta$-decay modes for nuclei across the nuclear chart. The $2\nu\beta\beta$ and $0\nu\beta\beta$ decays share initial and final states but differ on their momentum transfers (p) and intermediate states. Previous studies have found a correlation between the two $\beta\beta$-decay NMEs in ^{48}Ca [54] and a relation between their radial transition densities in all nuclei [55]. Also, $2\nu\beta\beta$-decay data is commonly used to adjust the proton-neutron quasiparticle random-phase approximation (pnQRPA) model parameters [56–60]. Here we perform systematic pnQRPA and nuclear shell model calculations, with various proton-neutron pairing strengths in the pnQRPA, and covering a wide range of nuclei and interactions in the shell model. Since $2\nu\beta\beta$-decay half-lives are known, a correlation between $\beta\beta$ NMEs can lead to $0\nu\beta\beta$-decay NMEs based on $2\nu\beta\beta$-decay data.

DOUBLE-BETA DECAY OPERATORS

The $2\nu\beta\beta$-decay half-life, to a very good approximation, depends on a single NME [60]:

$$M^{2\nu} = \sum_k \frac{(0_f^+ || \sum_a \tau_a^- \boldsymbol{\sigma}_a || 1_k^+)(1_k^+ || \sum_b \tau_b^- \boldsymbol{\sigma}_b || 0_i^+)}{(E_k - (E_i + E_f)/2 + m_e)/m_e}, \quad (1)$$

where indices a, b run over all nucleons, the isospin operator τ^- turns neutrons into protons, $\boldsymbol{\sigma}$ is the spin operator, and the denominator involves the energies E of the initial (i), final (f) and each kth intermediate 1^+ state. The electron mass m_e makes $M^{2\nu}$ dimensionless.

DOUBLE-BETA DECAY OPERATORS

For $0\nu\beta\beta$ decay, we focus on the best motivated light-neutrino exchange mechanism [3]. The decay rate is usually written in terms of a NME with three spin structures

$$M_{\rm L}^{0\nu} = M_{\rm GT}^{0\nu} - M_{\rm F}^{0\nu} + M_{\rm T}^{0\nu} \,, \tag{2}$$

called Gamow-Teller ($M_{\rm GT}^{0\nu}$), Fermi ($M_{\rm F}^{0\nu}$) and tensor ($M_{\rm T}^{0\nu}$) according to the operators $\mathcal{O}_{ab}^{\rm F} = \mathbb{I}$, $\mathcal{O}_{ab}^{\rm GT} = \boldsymbol{\sigma}_a \cdot \boldsymbol{\sigma}_b$, $\mathcal{O}_{ab}^{\rm T} = 3(\boldsymbol{\sigma}_a \cdot \hat{\mathbf{r}}_{ab})(\boldsymbol{\sigma}_b \cdot \hat{\mathbf{r}}_{ab}) - \boldsymbol{\sigma}_a \cdot \boldsymbol{\sigma}_b$ entering the definition

$$M_K^{0\nu} = \sum_{k,ab} \langle 0_f^+ || \mathcal{O}_{ab}^K \, \tau_a^- \tau_b^- \, H_K(r_{ab}) \, f_{\rm SRC}^2(r_{ab}) || 0_i^+ \rangle \,, \tag{3}$$

where r_{ab} is the distance between two nucleons. In the pnQRPA, we sum over all intermediate states, while in the shell model we directly compute NMEs between the initial and final states in the closure approximation. In both methods, $f_{\rm SRC}$ corrects for missing short-range correlations (SRCs) using two parametrizations [61]. The neutrino potentials are defined as

$$H_K(r_{ab}) = \frac{2R}{\pi g_{\rm A}^2} \int_0^\infty \frac{h_K \, j_\lambda(p\, r_{ab}) \, p^2 {\rm d}p}{\mathcal{E}_K} \,, \tag{4}$$

with $\mathcal{E}_K = p\,(p + E_k - (E_i + E_f)/2)$, $g_{\rm A} = 1.27$ and $R = 1.2A^{1/3}$ fm with nucleon number A. The spherical Bessel function j_0 enters all terms except the tensor where $\lambda = 2$. In the shell model, we use closure with two alternative denominators $\mathcal{E}_K = p(p + 1.12A^{1/2}{\rm MeV})$ [62] and $\mathcal{E}_K = p^2$ [31]. For the dominant GT term we have

$$h_{\rm GT} = g_{\rm A}^2(p^2) - \frac{g_{\rm A}(p^2) g_{\rm P}(p^2) p^2}{3m_{\rm N}} + \frac{g_{\rm P}^2(p^2) p^4}{12 m_{\rm N}^2} + \frac{g_{\rm M}^2(p^2) p^2}{6 m_{\rm N}^2} \,, \tag{5}$$

and other terms are defined likewise [17]. The leading parts are proportional to the axial coupling $g_{\rm A}(p^2)$—with dipole form factor [63]—and the pseudoscalar one $g_{\rm P}(p^2) = 2m_{\rm N} g_{\rm A}(p^2)(p^2 + m_\pi^2)^{-1}$. Here $g_{\rm M}$ is the magnetic coupling and $m_{\rm N}$, m_π the nucleon and pion masses.

Two-body currents

In addition to the standard shell-model and pnQRPA NMEs, we consider two additional contributions to $0\nu\beta\beta$ decay. First, we estimate the effect of two-body currents

$$\mathbf{J}^{\text{eff}}_{i,2\text{b}}(\rho,\mathbf{p}) = g_A\tau_i^- \left[\delta_a(p^2)\boldsymbol{\sigma}_i + \frac{\delta_a^P(p^2)}{p^2}(\mathbf{p}\cdot\boldsymbol{\sigma}_i)\mathbf{p}\right],$$

$$\begin{aligned}\delta_a(p^2) = &-\frac{\rho}{F_\pi^2}\left[\frac{c_4}{3}[3I_2^\sigma(\rho,p) - I_1^\sigma(\rho,p)]\right.\\ &-\frac{1}{3}\left(c_3 - \frac{1}{4m_\text{N}}\right)I_1^\sigma(\rho,p)\\ &\left.-\frac{c_6}{12}I_{c6}(\rho,p) - \frac{c_D}{4g_A\Lambda_\chi}\right],\end{aligned}$$

$$\begin{aligned}\delta_a^P(p^2) = &\frac{\rho}{F_\pi^2}\left[-2(c_3-2c_1)\frac{m_\pi^2 p^2}{(m_\pi^2+p^2)^2}\right.\\ &+\frac{1}{3}\left(c_3+c_4-\frac{1}{4m_\text{N}}\right)I^P(\rho,p)\\ &-\left(\frac{c_6}{12}-\frac{2}{3}\frac{c_1 m_\pi^2}{m_\pi^2+p^2}\right)I_{c6}(\rho,p)\\ &-\frac{p^2}{m_\pi^2+p^2}\left(\frac{c_3}{3}[I_1^\sigma(\rho,p)+I^P(\rho,p)]\right.\\ &\left.\left.+\frac{c_4}{3}[I_1^\sigma(\rho,p)+I^P(\rho,p)-3I_2^\sigma(\rho,p)]\right)\right.\\ &\left.-\frac{c_D}{4g_A\Lambda_\chi}\frac{p^2}{m_\pi^2+p^2}\right].\end{aligned}$$

with normal-ordered effective one-body currents [30]. This leads to the replacement

$$g_\text{A}(p^2,2\text{b}) \to g_\text{A}(p^2) + \delta_a(p^2)\,, \tag{6}$$

$$g_\text{P}(p^2,2\text{b}) \to g_\text{P}(p^2) - \frac{2m_\text{N}}{p^2}\,\delta_a^P(p^2)\,, \tag{7}$$

where δ_a, δ_a^P are the two-body corrections from Ref. [64], taken with uncertainties. They reduce β-decay NMEs by $20\% - 30\%$, thus contributing to their "quenching". Normal-ordered currents approximate well the full two-body β-decay results [29]. For more details on two-body currents, see Appendix A.

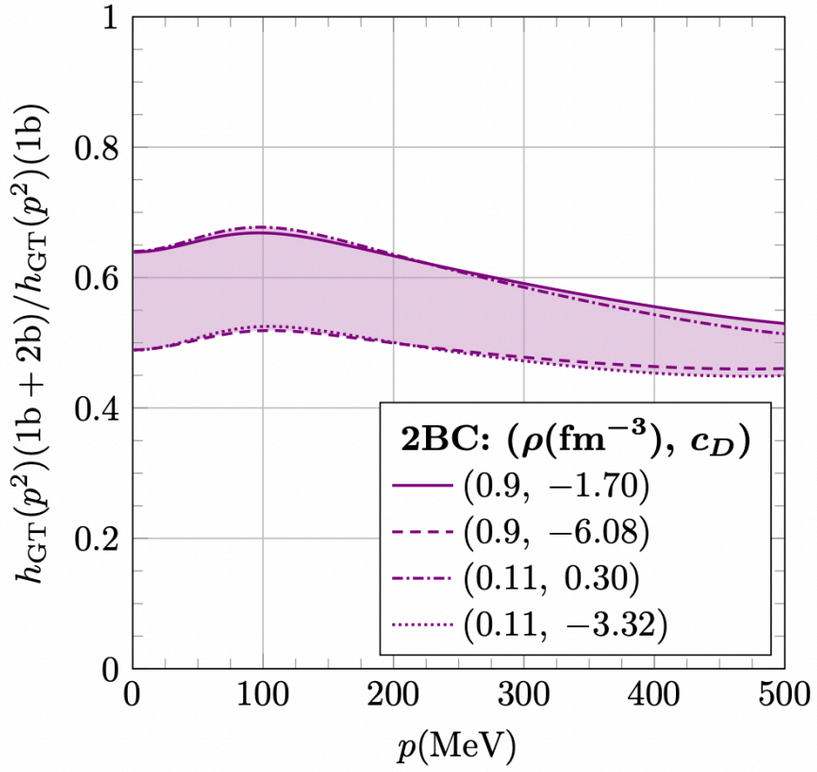

FIG. 5. Relative impact of two-body currents on the function $h_\text{GT}(p^2)$, with respect to the one-body values.

Two-body currents

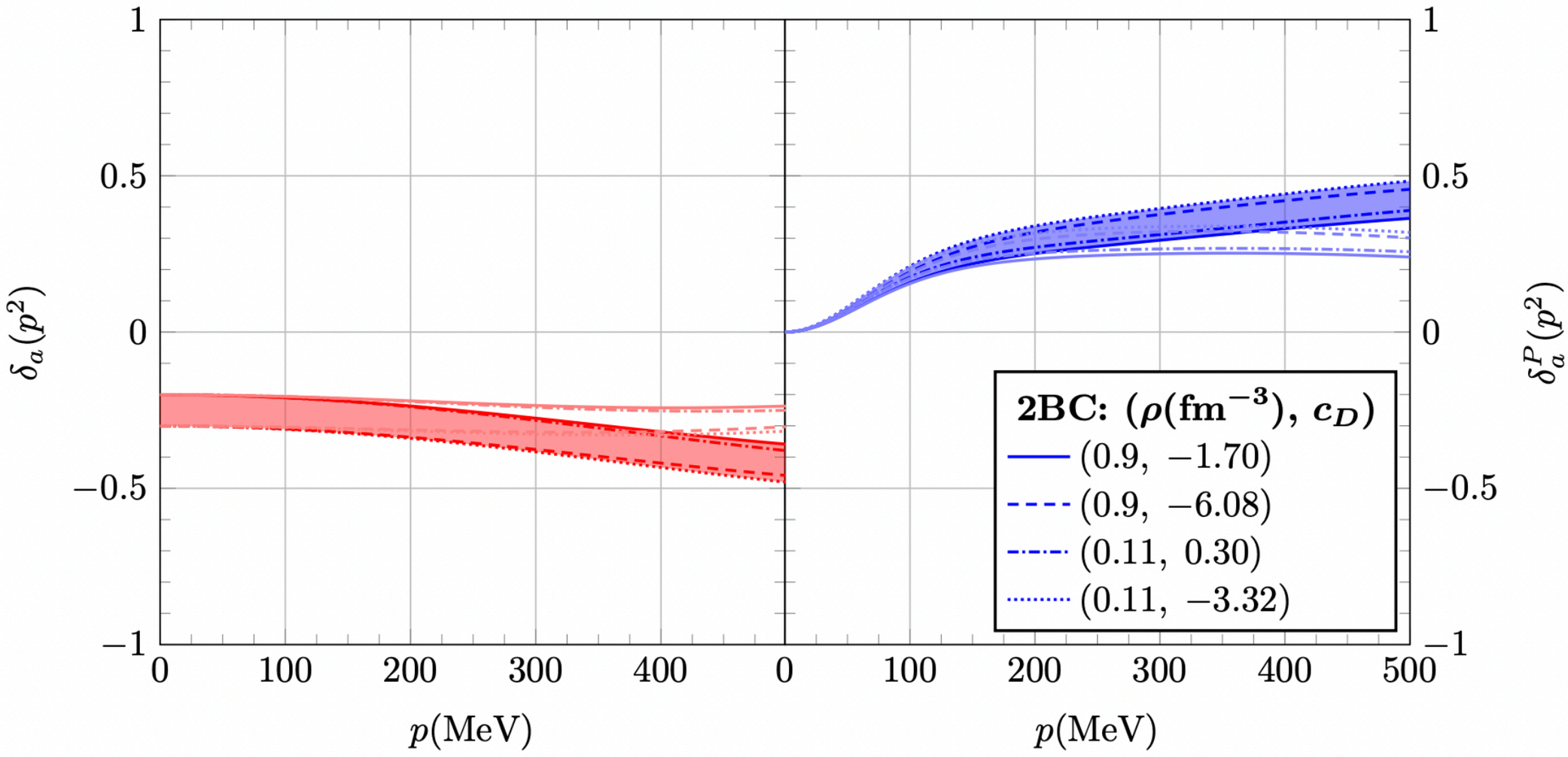

FIG. 6. Two-body contributions to axial (left) and pseudoscalar (right) currents. The open bands include a dipole regulator.

Short-range operator

Second, we also calculate the recently acknowledged short-range $0\nu\beta\beta$-decay NME [31], $M^{0\nu}_S$. This two-body term, obtained from Eq. (3) with $\mathcal{O}^{\rm S}_{ab} = \mathbb{I}$ but without summing over intermediate states, directly adds to the long-range part in Eq. (2). Because of its short-range character, it follows from $H_{\rm S}(r_{ab})$ in Eq. (4) with $\mathcal{E}^{0\nu}_{\rm S} = 1$ and j_0. We use

$$h_{\rm S} = 2g_\nu^{\rm NN} e^{-p^2/(2\Lambda^2)}\,, \tag{8}$$

with couplings $g_\nu^{\rm NN}$ and regulators Λ taken from the charge-independence-breaking terms of several nuclear Hamiltonians as in Ref. [36]. This approximates the two couplings entering $\beta\beta$ decay to be equal, which for ^{48}Ca gives a relative short-range NME contribution consistent with the *ab initio* result based on $g_\nu^{\rm NN}$ from QCD [35].

Many-body methods

We perform nuclear shell-model calculations for the decays of a large set of nuclei in the mass range $46 \leq A \leq 136$, covering three different configuration spaces with the following harmonic-oscillator single-particle orbitals—for both protons and neutrons—and isospin-symmetric interactions: i) $0f_{7/2}$, $1p_{3/2}$, $0f_{5/2}$, and $1p_{1/2}$ with the KB3G [65] and GXPF1B [66] interactions for the decay of $^{46-58}$Ca, $^{50-58}$Ti and $^{54-60}$Cr; ii) $1p_{3/2}$, $0f_{5/2}$, $1p_{1/2}$ and $0g_{9/2}$ with the GCN2850 [67], JUN45 [68] and JJ4BB [69] interactions for $^{72-76}$Ni, $^{74-80}$Zn, $^{76-82}$Ge and ^{82,84}Se; and iii) $1d_{5/2}$, $0g_{7/2}$, $2s_{1/2}$, $1d_{3/2}$ and $0h_{11/2}$ with the GCN5082 [67] and QX [70] interactions for $^{124-132}$Sn, $^{130-134}$Te and ^{134,136}Xe. We use the shell-model codes ANTOINE [71, 72] and NATHAN [72].

In addition, we study the decays of ^{76}Ge, ^{82}Se, ^{96}Zr, ^{100}Mo, ^{116}Cd, ^{124}Sn, ^{128,130}Te and ^{136}Xe with the spherical pnQRPA method. We use large no-core single-particle bases in a Coulomb-corrected Woods-Saxon potential [73] and obtain the BCS quasiparticle spectra for protons and neutrons separately. We use interactions based on the Bonn-A potential [74], with proton and neutron pairing fine-tuned to the empirical pairing gaps. For the residual interaction, we fix the particle-hole parameter to the GT giant resonance, and the isovector particle-particle one via partial isospin-symmetry restoration [59].

Many-body methods

As usual, we adjust the isoscalar particle-particle parameter to $2\nu\beta\beta$-decay half-lives. Additionally, we also explore an alternative approach and consider a range $g_{\rm pp}^{T=0} = 0.6-0.8$, which gives reasonable pnQRPA NMEs for β and $\beta\beta$ decays [58, 75].

Results

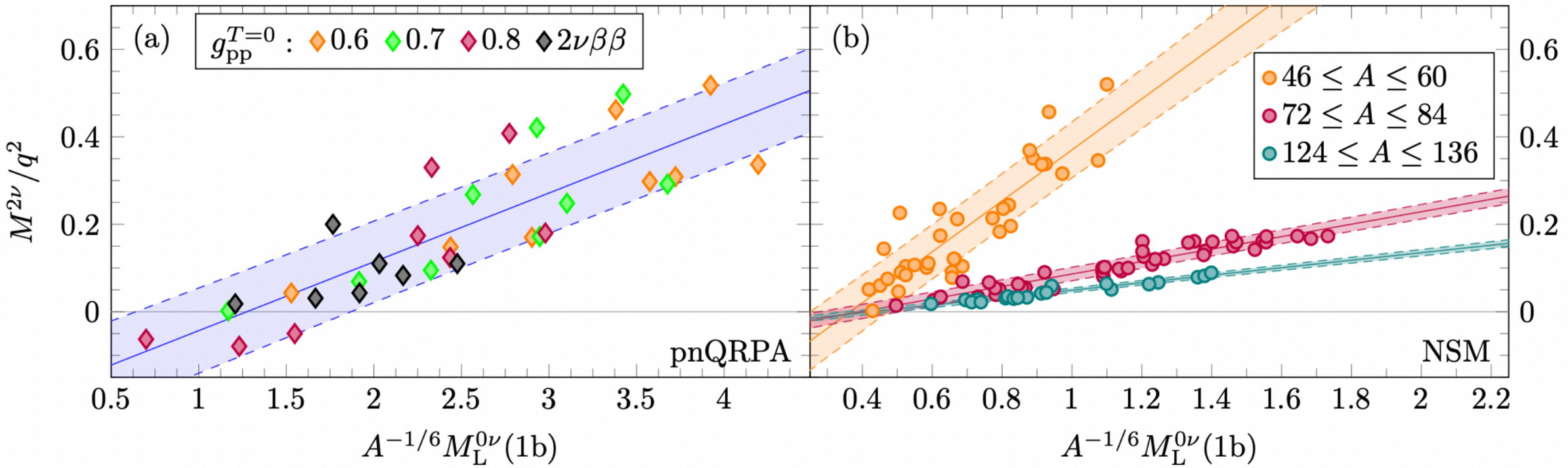

FIG. 1. $2\nu\beta\beta$- ($M^{2\nu}$) vs standard $0\nu\beta\beta$-decay ($M_L^{0\nu}$) NMEs obtained with (a) pnQRPA with different isoscalar pairing $g_{\rm pp}^{T=0}$ values (adjusted to $2\nu\beta\beta$-decay data for the black diamonds) and (b) nuclear shell model (NSM) with different interactions for three regions of the nucleon number A. $M_L^{0\nu}$ results are multiplied by $A^{-1/6}$, and the denominator q^2 notes the need to quench $M^{2\nu}$ values. Solid and dashed lines correspond to linear fits and their 68% CL prediction bands, respectively.

fit coefficients are $r = 0.84$ for the pnQRPA

for the shell model $r = 0.86$, $r = 0.95$ and $r = 0.97$
for the lighter, intermediate, and heavier nuclei, respec-

Results

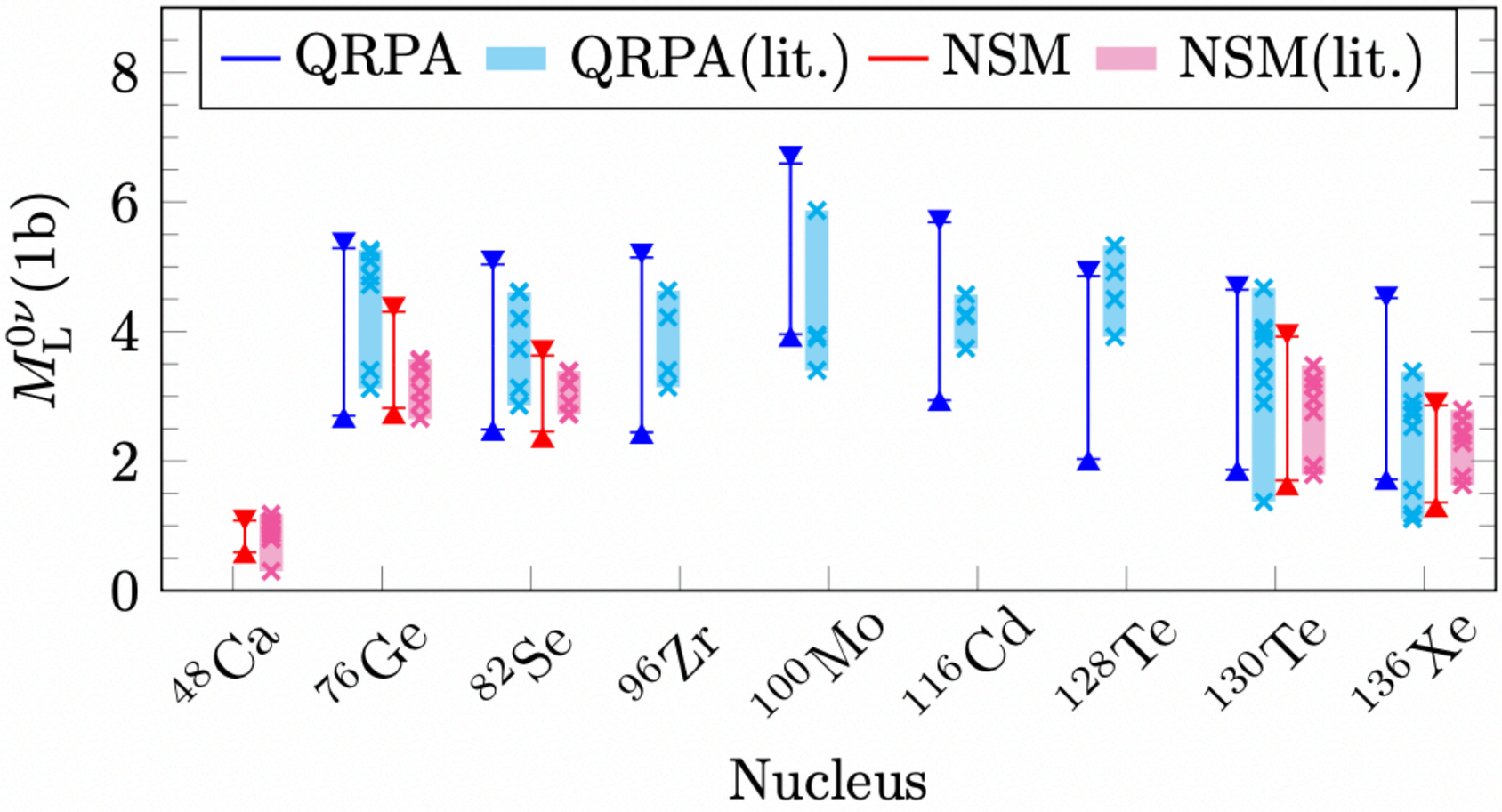

FIG. 2. Standard $0\nu\beta\beta$-decay NMEs obtained from the correlations in Fig. 1. The narrow error bars come from the 68% CL bands of the linear fits, while the wide ones also contain uncertainties in the NME calculations. Bands (crosses) show the literature NME ranges (individual values), shell model (NSM) in red [23–26, 36], QRPA in blue [36, 60, 77–80].

Two-body currents and short-range operator

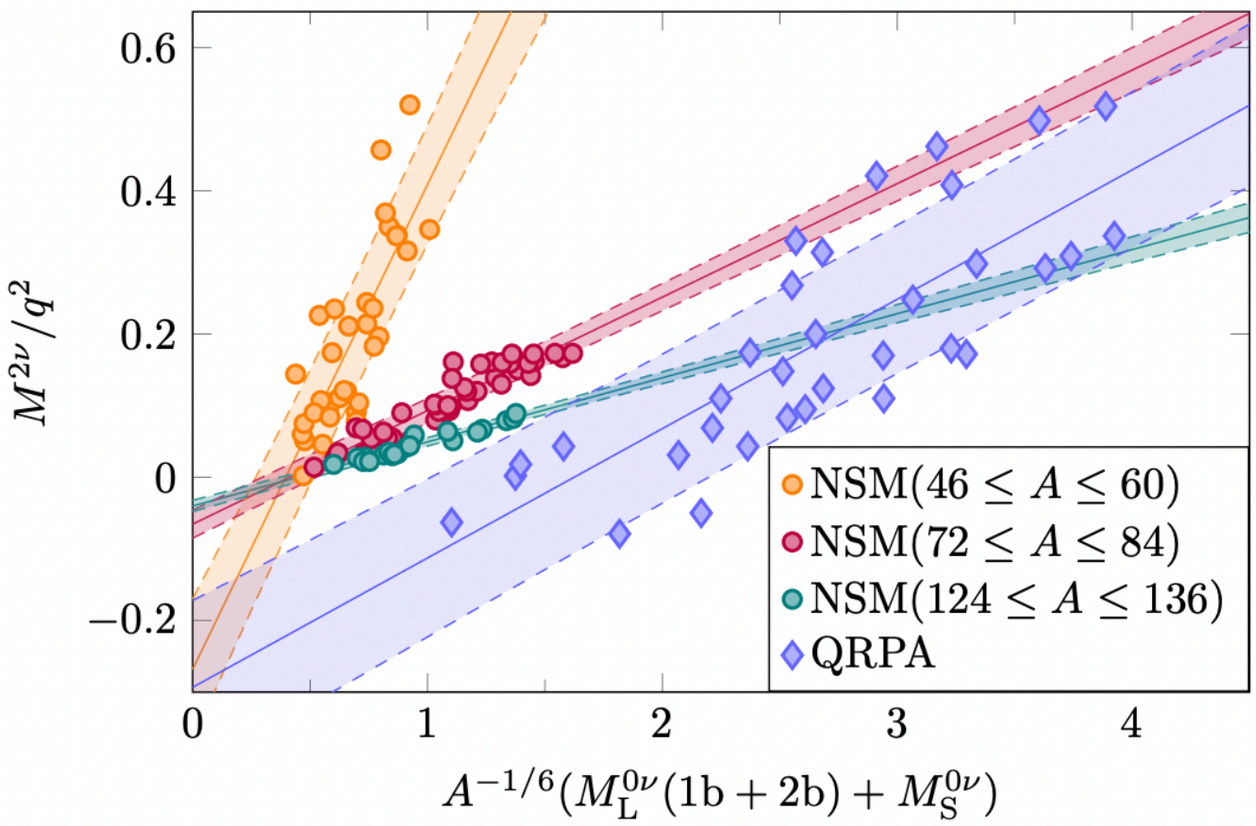

FIG. 3. $0\nu\beta\beta$- vs $2\nu\beta\beta$-decay NMEs and linear fits with 68% CL prediction bands for the shell model (NSM, circles) and pnQRPA (diamonds). The $0\nu\beta\beta$-decay results include two-body currents and short-range NMEs.

The effect of two-body currents on $0\nu\beta\beta$-decay NMEs is similar in the shell model and pnQRPA: NMEs decrease by $25\% - 45\%$. The range is mainly driven by the uncertainties in δ_a, δ_a^P. This reduction is somewhat larger than in earlier studies [30, 92] which neglect pion-pole diagrams [93]. In contrast to Ref. [30], the effect of

correlation coefficients become $r = 0.80$ in the pnQRPA and $0.81 \leq r \leq 0.97$ in the shell model (see Table I in Appendix B), smaller than in previous cases because the short-range term has Fermi spin structure, which does not contribute to $2\nu\beta\beta$ decay. Figure 3 also highlights

Finally, we add the short-range operator into $0\nu\beta\beta$-decay NMEs. In the pnQRPA, this term typically amounts to some $30\% - 80\%$ of the one-body $M^{0\nu}_{\mathrm{L}}$ value, and in the shell model this fraction is about $15\% - 50\%$. Individual uncertainties are now larger, dominated by the short-range coupling g_ν^{NN}. Figure 3 shows the corre-

Two-body currents and short-range operator

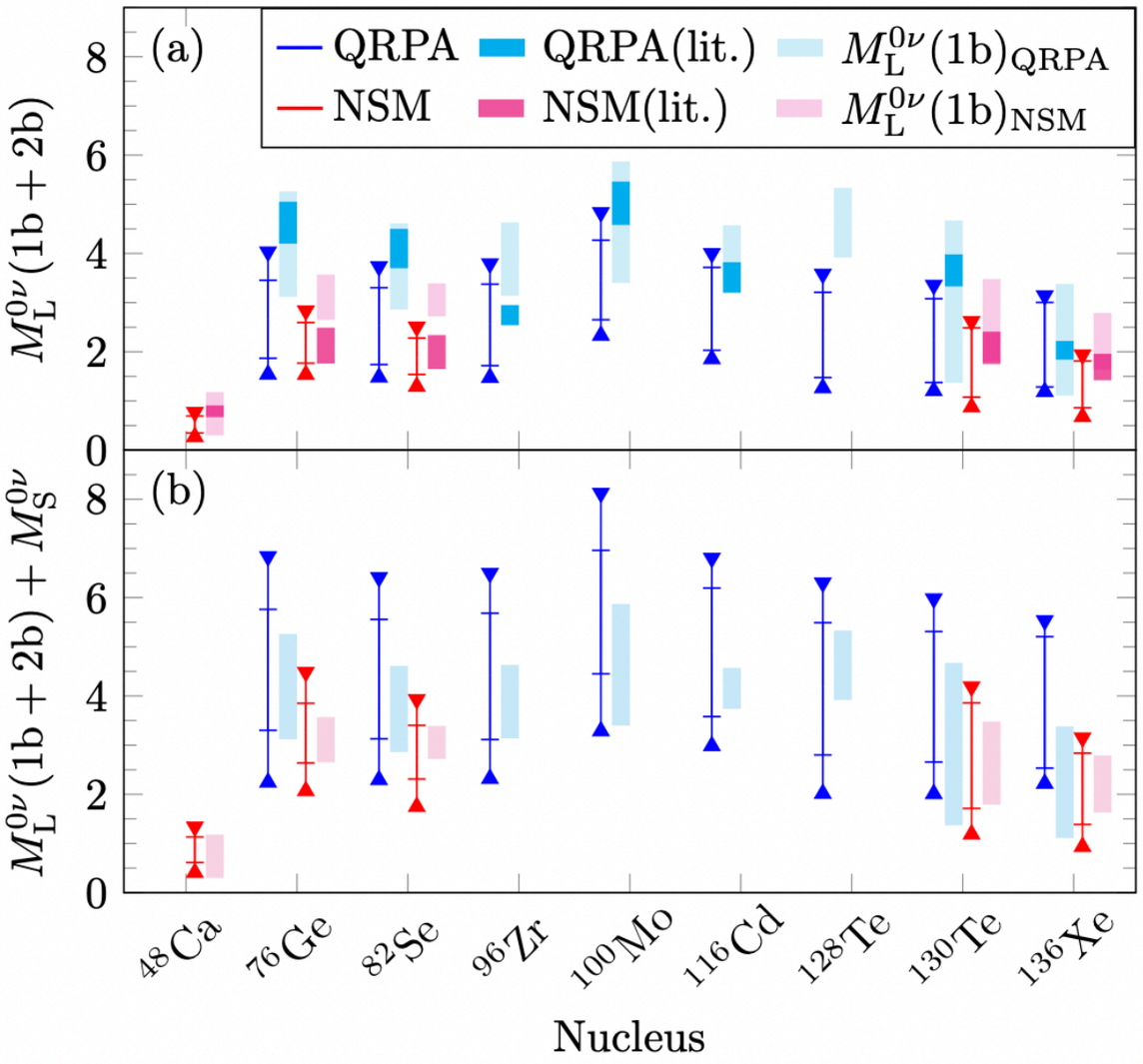

FIG. 4. $0\nu\beta\beta$-decay NMEs with error bars derived from correlation fits as in Fig. 2. (a) NMEs with two-body currents compared to Refs. [30, 92] (dark bands). (b) NMEs with two-body currents and the short-range term. For comparison, light bands show the literature bands of Fig. 2.

Our shell-model $M^{0\nu}_L(1b+2b)$ NMEs are in good agreement with *ab initio* results for ^{48}Ca [19–21] and ^{76}Ge [21] within uncertainties, and for ^{82}Se our error bar is just above the *ab initio* value [21]. This suggests that δ_a, δ^P_a effectively capture part of the missing many-body correlations—note that *ab initio* $0\nu\beta\beta$-decay NMEs do not include two-body currents yet. Further, our shell-model $M^{0\nu}_L(1b+2b)$ NMEs are consistent—with lower central values and larger uncertainties—with Ref. [94], which follows a different approach for adding correlations into the shell-model framework.

Summary

We perform shell-model and pnQRPA calculations for several tens of $\beta\beta$ decays and nuclear interactions and observe good linear correlations between $2\nu\beta\beta$- and $0\nu\beta\beta$-decay NMEs. We also find good correlations when including two-body currents and the short-range operator into $0\nu\beta\beta$ decay. Using the correlations and measured $2\nu\beta\beta$ decays, we obtain $0\nu\beta\beta$-decay NMEs with theoretical uncertainties based on systematic calculations following the same correlation, rather than individual NME results. Many-body approaches able to compute $2\nu\beta\beta$-decay NMEs [20, 21, 28] could pursue similar strategies to predict $0\nu\beta\beta$-decay NMEs with theoretical uncertainties.